Form Matters: Stable Helical Foldamers Preferentially Target Human Monocytes and Granulocytes

Form Matters: Stable Helix Foldamers Preferentially Target Human Monocytes and Granulocytes

Benedetta Del Secco,[a] Giulia Malachin,[b] Lorenzo Milli,[a] Nicola Zanna,[a] Emanuele Papini,[b] Andrea Cornia,[*c] Regina Tavano,[*b] Claudia Tomasini[* a]

[a] Dipartimento di Chimica Ciamician – Alma Mater Studiorum Università di Bologna – Via Selmi 2, 40126 Bologna (Italy); [b] Dipartimento di Scienze Biomediche – Università di Padova – Viale G. Colombo, 3 – 35121 Padova (Italy) [c] Dipartimento di Scienze Chimiche e Geologiche, Università di Modena e Reggio Emilia & INSTM – Via G. Campi 103 – 41125 Modena (Italy)

ABSTRACT: This work describes the preparation, the conformational analysis and the biological evaluation of some hybrid foldamers all containing the D-Oxd moiety alternated with a L-amino acid: while the cationic series contains both L-Val and L-Lys moieties, the neutral series contains only the small L-Ala moiety. The conformational analysis of all the oligomers suggested that only the longer oligomers of the L-Ala series fold into well-established helices, while the shorter oligomers containing L-Ala and all the oligomers of the cationic series give partially unfolded turn structures. All these molecules show a good biocompatibility, with no detrimental effects up to 64 μM concentrations.After equipping the foldamers with the fluorescent tag Rhodamine-B base, a quantitative analysis was obtained by dose and time response analysis by FACS of human HeLa cells, and primary blood lymphocytes, granulocytes and monocytes. Among the analyzed cells types, monocytes and granulocytes bind these oligomers with best efficacy, still visible after 24 h incubation. For the cationic foldamers the kinetics of cell association is slower than for the longer neutral versions. This outcome could be ascribed to the tendency of the latter ones to fold into stable helices, regardless of the presence of positive charges that can favor the cellular uptake.

INTRODUCTION

The understanding of sophisticated interplays between structure and function of molecules within complex systems is a great challenge in life sciences. Selective labeling of biomolecules with bio-physical probes in principle allows for investigation and manipulation of proteins, enzymes or biochemical processes in vitro as well as in vivo.[1] Various biological and biophysical methods may be used to study the internalization mechanism, to localize and to quantify the peptides internalization together with their cargoes inside cells. Yet, any method has its pitfalls, so a combination of different approaches is often needed to have access to the large pictures.

The fluorescence-based protocol requires the preparation of a peptide that is covalently coupled to a fluorophore. Its measurement by fluorescence (fluorimetry) enables the peptide indirect quantification and confocal microscopy allows its localization inside living cells.

Rhodamine dyes are well known synthetic molecules used for fabrics dyeing and belong to the class of xanthene dyes.[2] This fluorescent marker is used as fluorescent probe in biological studies, in structural microscopic studies, photosensitizers and laser dyes. It may be successfully introduced in synthetic structures,[3] called "foldamers".[4,5] This neologism refers mainly to medium-sized molecules (about 500–5000 Dalton) that fold into definite secondary structures (i.e., helices, turns and sheets), thus being able to mimic biomacromolecules despite their smaller sizes. Applications have ranged from cellular penetration [6] and membrane disruption to discrete molecular recognition,[7,8] while efforts to control the complex geometric shape of foldamers has entered the realm of tertiary and quaternary structures.[9,10]

Hybrid foldamers, containing the 4-carboxy-5-methyl-oxazolidin-2-one (Oxd) unit alternated with an α- or β-amino acid, have been extensively studied by our research group,[11] as the Oxd moieties impart rigidity to the peptide chain,[12–14] while the amino acids alternated with the D-Oxd moieties promote folding into well-established secondary structures.[15–17] In this work we describe the synthesis, the conformational analysis and the cellular uptake of a series of hybrid foldamers, all containing the D-Oxd unit alternated with an L-α-amino acid, to check any possible relationship between their preferred conformations and their behavior towards leukocytes. In the past, some studies of the Gellman group provided experimental support for the hypothesis that the formation of a globally amphiphilic helix is not required for host-defense peptide mimicry,[18] as also amphiphilic conformations of random copolymers without any helical structure were proven to exhibit potent antibiotic activity.

Our compounds have been synthesized in high yield and their preferred conformation has been analyzed with sev-

eral techniques both in solution and in the solid state. For the biological essays, the foldamers where further functionalized with Rhodamine B, that allows to measure their interactions with cells by fluorescence techniques.[19] For an efficient synthesis of all the conjugates, we developed a cheap and straightforward protocol to introduce Rhodamine B in a polypeptide chain, based on a microwave-assisted reaction.

RESULTS AND DISCUSSION

Foldamer synthesis

We prepared a series of oligomers with general formula HCl.H-(L-Xaa-D-Oxd)$_n$-L-Ala-Piperazine-Rhodamine B (Figure 1) with modification of either the foldamer skeleton or the chain length, to investigate whether the nature of the alternated L-amino acid modifies the foldamers preferred conformations, possibly affecting their cellular uptake.

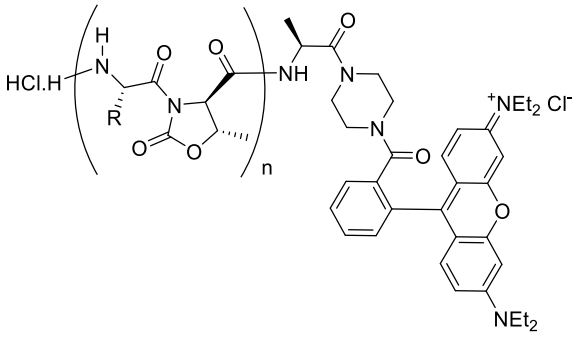

Figure 1. General structure of the foldamers prepared for the cellular uptake.

D-Oxd-OBn was obtained in high yield starting from D-threonine in multigram scale,[17] and coupled with protected L-valine or L-lysine in the presence of HBTU and DIEA to prepare **1** and **2** that are used to access complex foldamers (Schemes 1 and 2, for all the synthetic details, see SI). These amino acids have been chosen as they have very different polarity, being L-Val a neutral and highly branched amino acid, while L-Lys is a basic and hydrophilic amino acid. These moieties have been extensively used in the preparation of antimicrobial peptides,[18,20,21] as they may furnish to the backbone a lipophilic chain alternated with a cationic chain, that are both needed to cross the microbial cell membrane.[18]

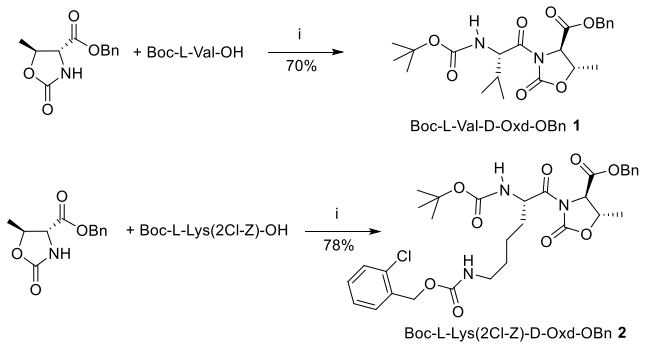

Scheme 1. Reagents and Conditions: (i) HBTU (1.1 equiv.), Et_3N (2 equiv.), dry CH_3CN, 1 h, r.t.

Compound **2** was prepared using Boc-L-Lys(2Cl-Z)-OH, as the 2Cl-Z group is stable towards hydrogenolysis under mild conditions (Scheme 1). Complex foldamers **3**, **5** and **7** and the corresponding fully deprotected oligomers **4**, **6** and **8** have been prepared in solution alternating the hydrophilic and the lipophilic moieties with high yields (Scheme 2). For the biological essays of compounds **4**, **6** and **8** chloride counterions are needed, so the usual deprotection strategy based on trifluoroacetic acid was replaced with a protocol envisaging hydrochloric acid,[22] that afforded fully deprotected oligomers as hydrochloride salts in high yield.

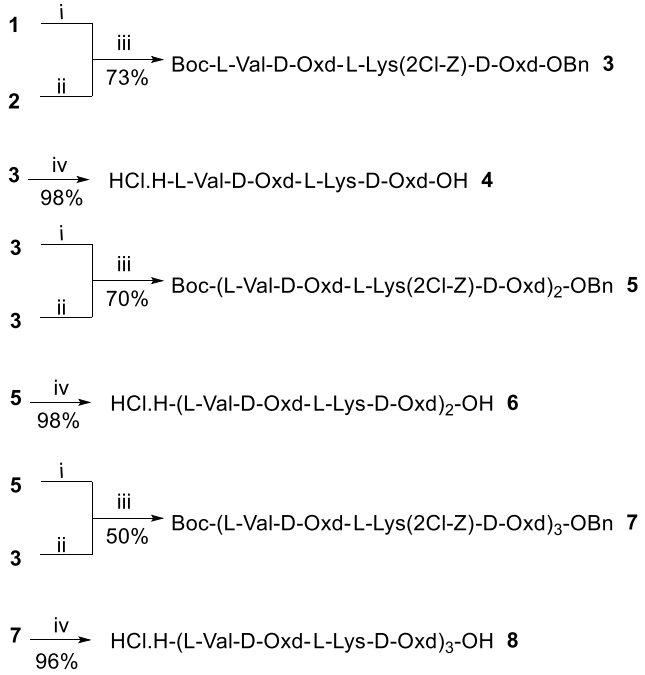

Scheme 2. Reagents and Conditions: (i) H_2, Pd/C (10%), MeOH, r.t., 16 h; (ii) TFA (18 equiv.), dry CH_2Cl_2, r.t., 4 h; (iii) HBTU (1.1 equiv.), Et_3N (2 equiv.), dry CH_3CN, 1 h, r.t.; (iv) Pd/C (10%), 11 M HCl, dry MeOH, 4 h, r.t; then 2,2,2-trifluoroethanol, dry CH_2Cl_2, 3 h, r.t.

To cross-check our interpretation, we have synthesized the fully deprotected foldamers HCl.H-(L-Ala-D-Oxd)$_n$-OH (n = 2, 4, 6, 8) **9**, **10**, **11** and **12**, which contain neither

sterically demanding residues nor functionalized side-chains.

Foldamers Biocompatibility Evaluation

The biocompatibility of fully deprotected oligomers of both series was checked. HeLa cells were seeded and incubated for 24h with compounds **4**, **6**, **8**, **9**, **10**, **11** and **12** at different concentrations, then cells were washed, MTS solution was added and the absorbances were read by an ELISA reader after 30 minute incubation. All tested oligomers have demonstrated to be non-toxic up to 64 μM and after a 24 hours incubation to HeLa cells, as assayed by MTS test, irrespective of length and charge (Figure 7). This outcome suggests a good biocompatibility of our foldamers formulations.

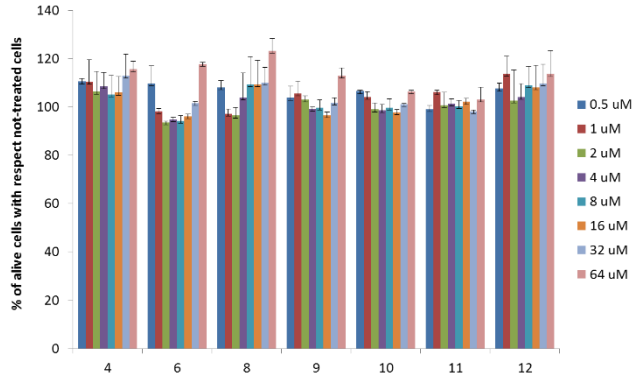

Figure 7. MTS assay performed on the fully deprotected foldamers HCl.H-(L-Val-D-Oxd-L-Lys-D-Oxd)$_n$-OH **4**, **6** and **8** and HCl.H-(L-Ala-D-Oxd)$_n$-OH **9**, **10**, **11** and **12**. Percentage of alive cells were obtained with respect to control cells. Results are representative of one experiment run in triplicate.

Synthesis of the Rhodamine Containing Oligomers

Usually fluorescently labelled peptides or foldamers are prepared by reaction of *N*-deprotected oligomers with fluorescein isothiocyanate,[48] a readily available although quite expensive reagent. We developed a new method to prepare a derivative of the cheap Rhodamine B base that may be easily used to prepare fluorescent bioconjugates. By modification of a well known procedure,[49,50] we added Rhodamine B base to piperazine-trimethyl aluminium in toluene (Scheme 3). The reaction mixture was stirred under microwave irradiation at 50 W for 1 h, then acidified, filtered and purified by crystallization. The resulting derivative piperazine-Rhodamine B 13 was obtained in excellent yield and was then coupled with Boc-L-Ala-OH in the presence of HATU e DIEA in high yield to afford pure Boc-L-Ala-Piperazine-Rhodamine B 14 after flash chromatography.

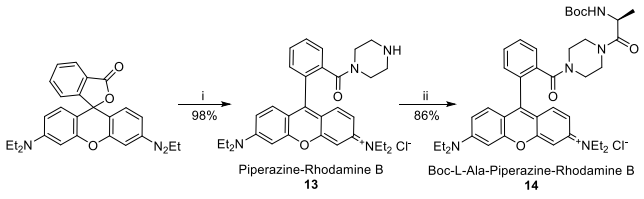

Scheme 3. Reagents and Conditions: (i) $AlMe_3$ (2 equiv.), piperazine (4 equiv.), toluene, MW 50W, 1h; (ii) Boc-L-Ala-OH (1 equiv.), HATU (1.1 equiv.), DIEA (2 equiv.), dry acetonitrile, 1 h, r.t.

To gain deeper insight into the influence of foldamer nature (preferred conformation, charge, length, etc.) on cellular uptake, five foldamers have been chosen to be coupled with **14** by straightforward peptide coupling reactions described in Scheme 4. The synthetic pathway for the preparation of fluorescent foldamers **16**, **18**, **20**, **22** and **24** is reported in Scheme 4.

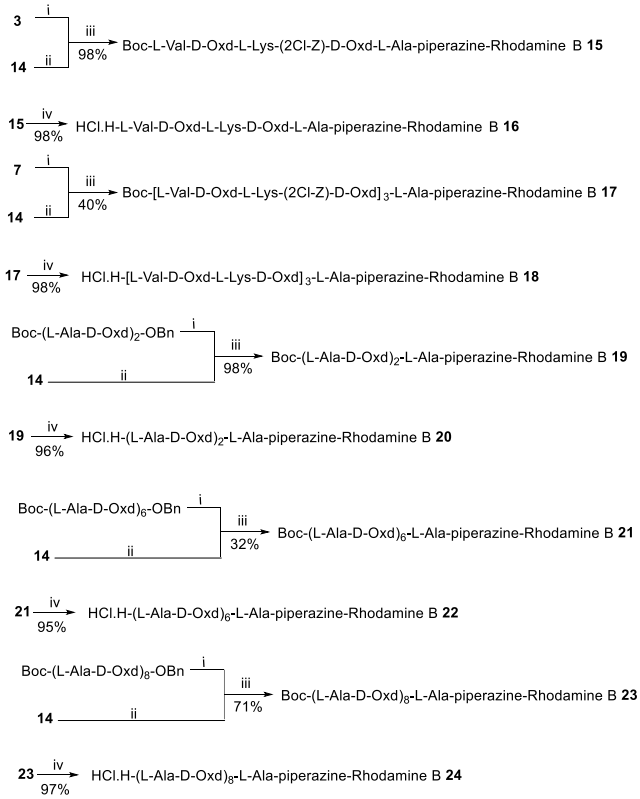

Scheme 4. Reagents and Conditions: (i) H_2, Pd/C (10%), AcOEt, r.t., 2 h ; (ii) TFA (18 equiv.), dry CH_2Cl_2, r.t., 4 h; (iii) HATU (1.1 equiv.), DIEA (3 equiv.), dry CH_3CN, 1 h, r.t.; (iv) H_2, Pd/C (10%), 12M HCl (4 equiv.), AcOEt, r.t., 2 h.

Biological Evaluation of the Rhodamine Containing Foldamers

The qualitative analysis was performed with human monocytes purified from buffy coats of healthy donors, seeded and incubated for 18 h with selected foldamers at different concentrations.

Confocal microscopy analysis of cells incubated with the Rhodamine-conjugated foldamers indicates that all the analyzed Rhodamine-labelled analogues of neutral and cationic foldamers are readily captured by monocytes and internalized in endocytic vesicles (all the results are shown in Figure S9), although the best result is obtained with 22 (Figure 8). Confocal analysis indicates that cells,

although not affected by oligomers, can capture them. The cytosolic distribution of the fluorescence signal of labelled analogues is punctuated and clearly reminiscent of an endocytic mechanism of cell accumulation in monocytes.

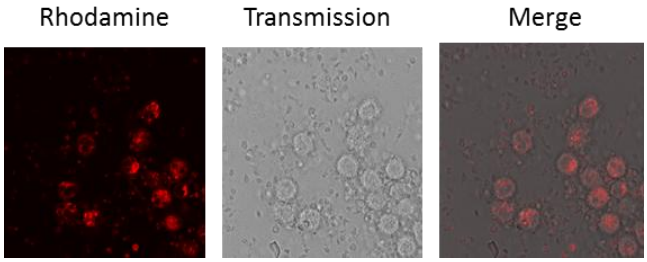

Figure 8. Confocal analysis of human monocytes after purification from buffy coats of healthy donors, seeding and incubation for 18h with **22** (20 μM). The cells were washed with PBS and directly analyzed by confocal microscopy.

After this qualitative analysis, a quantitative analysis of all the oligomers was carried out by a dose and time response analysis by Fluorescence Activated Cell Sorting (FACS) of primary human blood cells (lymphocytes, granulocytes and monocytes) and the tumor derived non-leukocyte human cell line HeLa (human ovary sarcoma). Purified human lymphocytes, granulocytes and monocytes and HeLa cells were incubated for 3 hours or 24 hours with foldamers **16**, **18**, **20**, **22** and **24** (Table 2), together with L-Ala-Piperazine-Rhodamine B as a comparison (Figure S10). The cells were then washed with PBS, recovered and directly analyzed by cytofluorimetry. Both the cell capture efficacy and the selectivity are modulated by length, charge and conformation of the foldamers. In the case of the $(L\text{-}Ala\text{-}D\text{-}Oxd)_n$ series, **22** shows the best cell association after a 3 h incubation, followed by **24**, while **20** is captured only slightly more than the background (estimated by cell association of simple Rhodamine dye, see Figure S10). Monocytes and granulocytes are targeted more effectively than HeLa cells and lymphocytes both by **22** and by **24**. Such a cell-binding pattern is maintained also after 24 h incubation. Collectively data indicate that **22** is taken up by cells better than shorter **20** or longer **24** analogues and can preferentially target blood myeloid cells (monocytes and granulocytes) than lymphoid and epithelial cells.

Since cells have a negative superficial charge, we studied the effect of a Lys residue in the structure of foldamers **16** and **18** of the $(L\text{-}Val\text{-}D\text{-}Oxd\text{-}L\text{-}Lys\text{-}D\text{-}Oxd)_n$ series. The introduction of a positively-charged moiety in the sequence of **16** increases cell capture compared to **20**, although with a slow kinetics, being the improvement better visible after 24 h than after 3 h. In contrast, the introduction of three positive charges in foldamer **18** decreases its cell capture efficacy compared to **22**, and this effect is marked after short incubation time. In both cases the kinetics of cell association was slower that for neutral versions, reaching higher values after 24 h incubation. Cell selectivity remained the same as for neutral foldamers.

Table 2. Association of foldamers 16, 18, 20, 22 and 24 to different human cells after 3 hours incubation (left) and after 24 hours incubation (right). Results are representative of one experiment run in duplicate. MFI: mean fluorescence intensity.

Foldamer	After 3 hours	After 24 hours
16	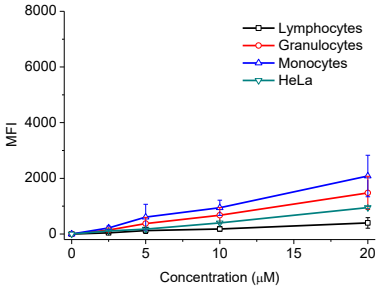	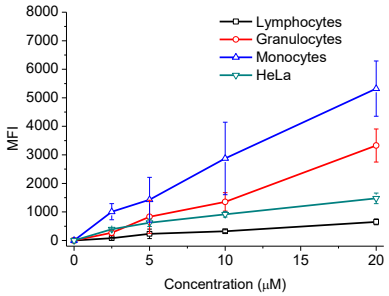
18	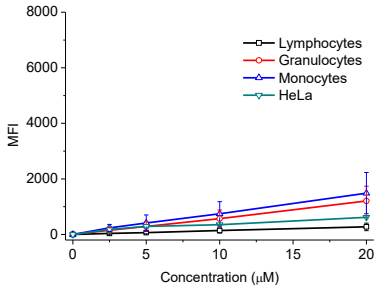	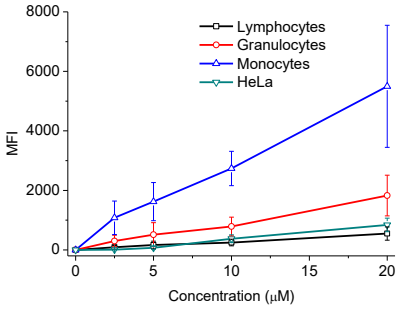
20	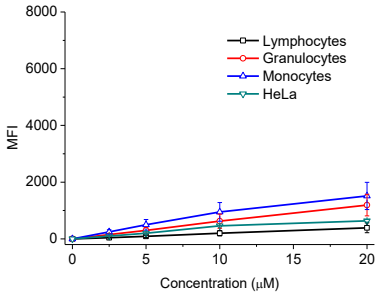	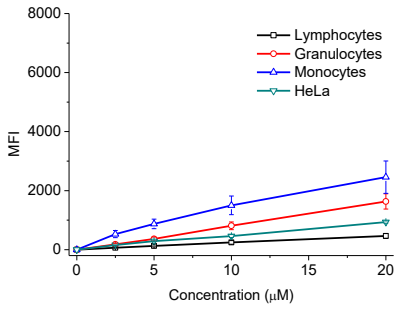
22	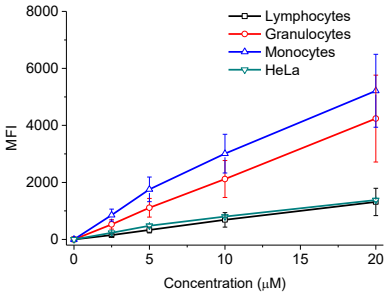	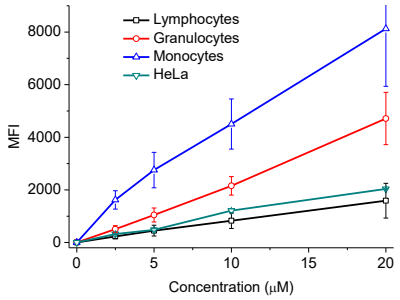
24	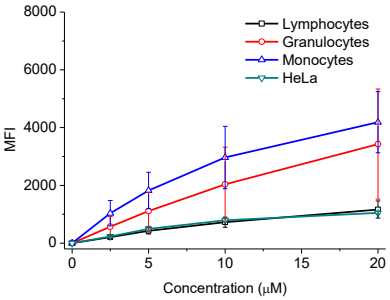	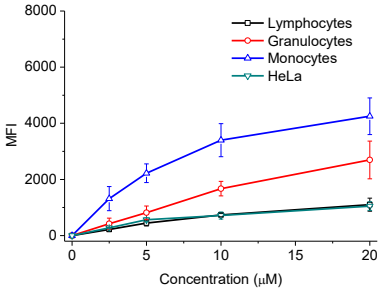

Conformational Analysis

The preferred conformation of the oligomers **3**, **5** and **7** of increasing length was analyzed by FT-IR, ^{1}H NMR and ECD spectroscopy. Only the shortest oligomer **3** was obtained as crystals of sufficient quality for a single-crystal X-ray diffraction investigation (see below).

FT-IR spectroscopy analysis in solution helps detecting the formation of intramolecular N-H•••O=C hydrogen bonds. Non-hydrogen-bonded amide N-H groups exhibit a stretching signal above 3400 cm^{-1}, while hydrogen-bonded groups produce a stretching band below 3400 cm^{-1} (Figure 2a).[23] All studied foldamers feature free N-H amide groups in CH_2Cl_2 solution. However, when moving from **3** to **7**, the amount of intramolecular N-H•••O=C hydrogen bonds increases as shown by a broad band centered at about 3250 cm^{-1}. Such a band is totally absent in the spectrum of **3**, is weak in **5** and becomes dominant in **7**. The carbonyl stretching bands are in agreement with this trend (Figure 2b). The spectrum of **7** shows a strong band at 1665 cm^{-1}, typical of hydrogen-bonded carbonyl groups. A weak band at the same wavenumber may be found also in the spectrum of **5**, while it is totally absent in **3**. These results suggest that the shortest oligomer **3** is not organized in secondary structures and the organization rises as the chain length increases.

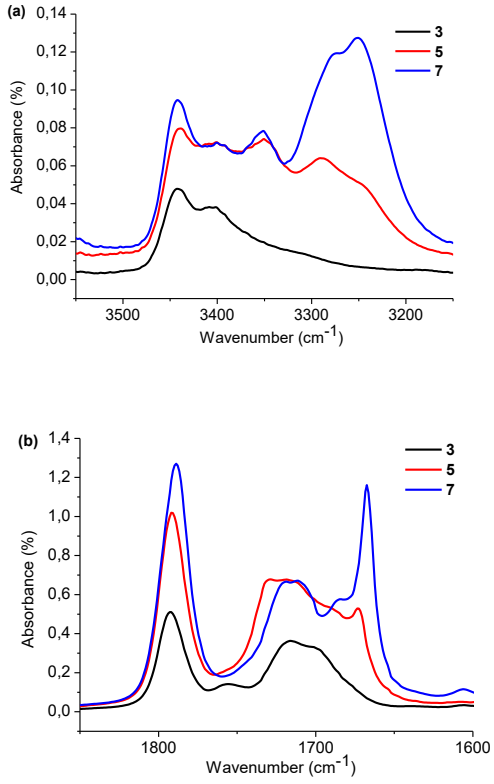

Figure 2. (a) N-H and (b) C=O stretching regions of the IR absorption spectra of oligomers **3**, **5**, and **7** in CH_2Cl_2 solution (3 mM, room temperature).

A confirmation of these results was obtained by investigating the DMSO-d_6 dependence of NH proton chemical shifts in NMR spectra.[24] DMSO is a strong hydrogen bond acceptor and causes a considerable downfield shift of the proton signal when bound to a free NH proton.[25] In Table 1 we present the results of such an analysis for foldamers **3**, **5** and **7** in the form of chemical shift variations ($\Delta\delta$) upon NH titration with DMSO-d_6 (the interested reader may consider Figure S1). The NH-Boc and NH-2Cl-Z groups, whose NH chemical shifts lie at about 5-6 ppm,[26] are omitted as scarcely informative, moreover the NH-2Cl-Z groups would not be involved in the helix formation. Compounds **3** and **5** give large $\Delta\delta$ values of about 1 ppm, suggesting that their NH hydrogens are not involved in intramolecular H-bonding. By contrast, the five NH groups of longer foldamer **7** are less sensitive to DMSO-d_6 addition and display moderately to strongly reduced $\Delta\delta$ values (0.77 to 0.33 ppm). Thus, according to both NMR and IR spectroscopies **7** entails the largest proportion of intramolecularly H-bonded NH groups. Notice, however, that solution IR spectra (Figure 2) point to the presence of free NH amide groups in *all* studied foldamers *plus* H-bonded NH's in **5** and, to a greater extent, in **7**, thus confirming that molecules tend to form a folded structure but with some remaining equilibria between folded and unfolded conformations.

ROESY analysis of **7** in $CDCl_3$ (Figure S2) showed no NH-NH cross peaks typical of helical secondary structures.

Table 1. $\Delta\delta$ (ppm) for amide-NH titration in foldamers 3, 5 and 7.

Compound	NH(1)	NH(2)	NH(3)	NH(4)	NH(5)
3	0.95				
5	0.97	0.95	0.98		
7	0.77	0.67	0.36	0.38	0.33

Unfortunately, the electronic circular dichroism (ECD) spectra of **3**, **5** and **7** are not very informative due to the presence of the protecting aromatic groups, so ECD was used to pursue conformational studies on the fully deprotected foldamers **4**, **6** and **8** in water solution (3 mM) at room temperature.

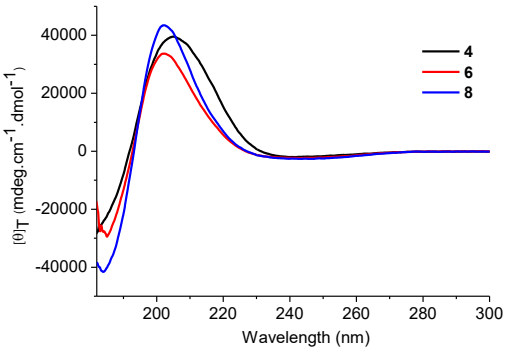

Figure 3. Normalized *per*-residue ECD spectra of compounds **4**, **6** and **8** in H_2O solution (3 mM, room temperature).

The *per*-residue ECD spectra of the three compounds (Figure 3) are nearly superimposable and display a strong negative signal at 182-185 nm, a positive band at 202-204 nm, and finally a broad and weak negative band centered at 242 nm. The modest variations among the three spectra suggest that the longer oligomers do not assume a helix conformation but rather fold in a turn conformation.[27] Unlike the α-helix and β-sheet, there is no unique ECD signature for turns because of the range of conformers included in this structural category.[28] Various spectral patterns were predicted, but the predominant one had a weak negative $n \rightarrow \pi^*$ band at 220–230 nm and two strong $\pi \rightarrow \pi^*$ bands, a positive one at 200–210 nm and a negative one at 180–190 nm.[29] The turn preferred conformation may be attributed to the presence of sterically demanding residues with β-branched side chains or to residues which can form side-chain to main-chain intra-strand H-bonds.

The ECD spectra of the the fully deprotected foldamers HCl.H-(L-Ala-D-Oxd)$_n$-OH (n = 2, 4, 6, 8) **9**, **10**, **11** and **12**, recorded in the same experimental conditions as Figure 3, are presented in Figure 4. The spectra of the shorter oligomers **9** and **10** are similar to those of the HCl.H-(L-Val-D-Oxd-L-Lys-D-Oxd)$_n$-OH series, with a strong negative signal at 185 nm, a positive band at 201 nm and a broad negative band centered at 230 nm.

In contrast, the spectrum of **11** displays a strong positive signal at 193 nm and two negative bands centered at 208 and 228 nm respectively, with $R = [\theta]_{228}/[\theta]_{208} = 0.75$, like the parent Boc-(L-Ala-D-Oxd)$_6$-OH.[15] This is the typical ECD signature of 3_{10} helices, in agreement with the work of Toniolo and coworkers [30,31] and with theoretical calculations.[32] Both experimental and theoretical studies point to the following main characteristics of the 3_{10}-helix: (a) a negative ECD band centred near 207 nm; (b) a negative shoulder in the vicinity of 222 nm; (c) a $R = [\theta]_{222}/[\theta]_{207}$ ratio smaller than the value reported for the α-helical peptides, that usually exhibit an R of about 1; (d) a positive maximum al 198 nm.

Finally the longer foldamer **12** displays the ECD spectrum characteristic of an α-helix, with a negative band at 226 nm attributable to the $n \rightarrow \pi^*$ transition of the peptide group. The peptide $\pi \rightarrow \pi^*$ transition gives rise to the remaining two bands, through exciton splitting: the negative band at 201 nm (parallel exciton band) and the positive band at 188 nm (perpendicular exciton band). In this case the $R = [\theta]_{226}/[\theta]_{201}$ ratio is 0.85.

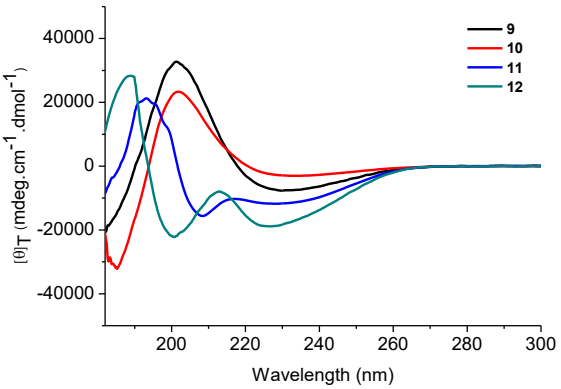

Figure 4. Normalized *per*-residue ECD spectra of compounds **9**, **10**, **11** and **12** in H_2O solution (3 mM, room temperature).

From the ECD analysis we could demonstrate that all cationic foldamers and the short neutral ones have the same ECD signature, suggesting that they assume a rather unfolded conformation, while the longer neutral foldamers show spectra typical of helices. To probe the conformation of these materials in the solid state, we tried to crystallize foldamers of the two series in both protected and deprotected forms. Since it is known that crystallization is more difficult for enantiomerically pure chiral molecules than for the corresponding racemates,[33–36] we also synthesized enantiomers and prepared racemates. It is still not clear whether more facile crystallization of racemic protein mixtures is a general phenomenon,[37] but racemic crystallization has been extensively studied for proteins, short peptides[38] and DNA.[39] Recently, this technique and X-ray crystallography have been successfully applied to the determination of the unknown structure of snow flea antifreeze protein (sfAFP),[40] and of the crystal structures of seven tripeptides in enantiomeric and racemic forms.[41]

After several attempts, X-ray quality crystal of *rac*-Boc-L-Ala-D-Oxd-OBn, Boc-(D-Ala-L-Oxd)$_2$-OBn and Boc-L-Val-D-Oxd-L-Lys(2Cl-Z)-D-Oxd-OBn (**3**) were grown by slow evaporation of ethyl acetate or chloroform solutions. Crystals of Boc-(D-Ala-L-Oxd)$_2$-OBn were obtained from the racemate and spontaneous resolution thus occurred during crystallization (see Experimental Section for details on absolute structure determination). Unfortunately we were not able to grow suitable crystals of the longer foldamers. The molecular structures of Boc-L-Ala-D-Oxd-OBn, Boc-(L-Ala-D-Oxd)$_2$-OBn and **3** are depicted in Figures 5 and 6 (for an easier comparison, we show enantiomers with the same absolute configuration at corresponding chiral centers). Additional plots of molecular and crystal structures are provided as Figures S3-S8. All crystal data and refinement parameters are given in Table S1 while the geometry of hydrogen-bond interactions and conformational data are gathered in Tables S2-S4 and S5-S7, respectively.

In the solid state, the three compounds do not form *intra*molecular N-H····O=C hydrogen bonds. Amide nitrogen atoms are involved only in *inter*molecular hydrogen bonds or in no H interaction at all, like for the amide nitrogen N1 in Boc-(D-Ala-L-Oxd)$_2$-OBn. The emerging picture thus agrees well with solution IR and NMR data (see above and Ref. 15). Secondary structure relies just on C-H···O interactions: in the three studied foldamers, the α-carbon atom of each amino acid residue has an H contact with the endocyclic carbonyl oxygen of the neighboring Oxd moiety (see legend to Figures 5 and 6 for details). Such a nonclassical hydrogen bond is commonplace in the solid state structure of Oxd-based foldamers[11,15,42,43] and persists in solution, as judged by the chemical shift of α-protons in NMR spectra.[14,15,17,44]

Turning now to intermolecular interactions in the solid state, the crystal lattice of *rac*-Boc-L-Ala-D-Oxd-OBn entails centrosymmetric supramolecular dimers held together by a pair of N-H···O=C bonds between the two antiparallel peptide segments, with HN1···O1' = 2.305(16) Å and N1-HN1···O1' = 156.7(13)° (Figure S4). Molecules of Boc-(D-Ala-L-Oxd)$_2$-OBn and **3** are arranged in chains that run parallel to the **b** axis and are generated by the 2_1 screw axis (Figures S6 and S8). In the two compounds, a classical H-bond is formed between the amide nitrogen N3 and carbonyl oxygen O2 of the same peptide segment, but belonging to a neighboring, antiparallel molecule in the chain, with HN3···O2' = 2.05(2)/1.914(18) Å and N3-HN3···O2' = 160(3)/173(2)° in Boc-(D-Ala-L-Oxd)$_2$-OBn/**3**. In Boc-(D-Ala-L-Oxd)$_2$-OBn, the carbonyl oxygen O3 is engaged in a further H-contact along the chain with the L-Oxd1 tertiary carbon C17 (H17'···O3 = 2.38 Å, C17'-H17'···O3 = 135.1°). A similar chain-like supramolecular arrangement based on a single classical H bond was previously found in Boc-(L-Phe-D-Oxd)$_n$-OBn, the alignment of peptide units being parallel and antiparallel for n = 1 and 2, respectively.[45,46] The two remaining amide nitrogens N1 and N5 of **3** are engaged in further contacts along the chain with one oxygen atom of the 2Cl-Z group (HN1···O12' = 2.305(18) Å, N1-HN1···O12' = 165(2)°) and carbonyl oxygen O1 (HN5'···O1 = 2.171(17) Å, N5'-HN5'···O1 = 172(2)°), respectively. Finally, a C-H···O contact occurs between the D-Oxd2 tertiary carbon C7 and the D-Oxd1 endocyclic carbonyl oxygen O9 (H7···O9' = 2.35 Å, C7-H7···O9' = 157.6°). The three compounds entail many other C-H···O contacts with H···O > 2.3 Å which provide potential nonclassical H bonds of both intra- and intermolecular nature (Tables S2-S4).

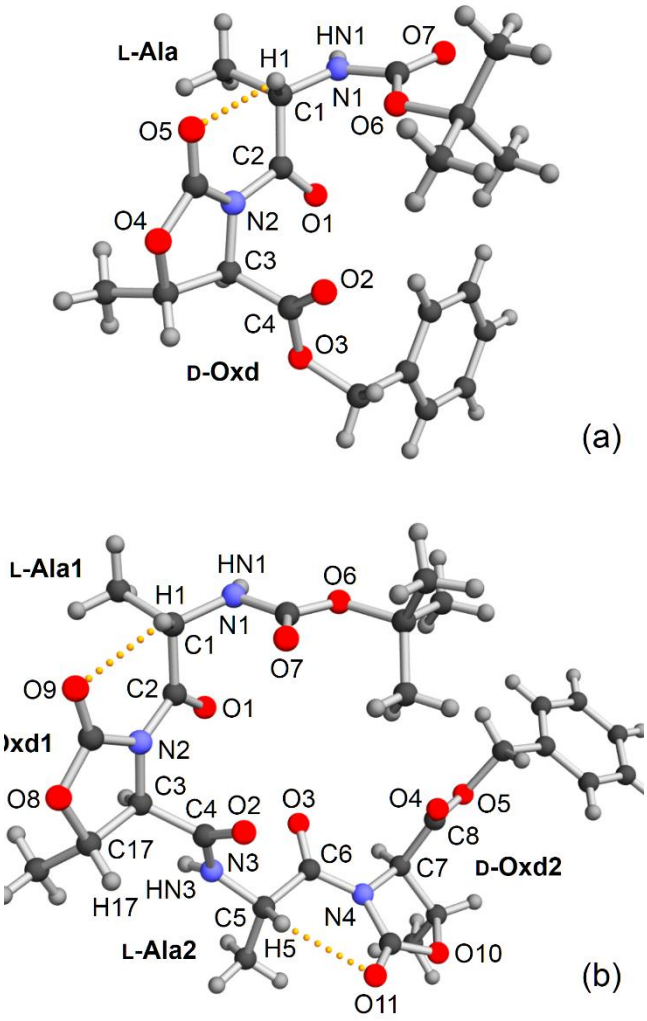

Figure 5. Molecular structure of (a) Boc-L-Ala-D-Oxd-OBn molecule in *rac*-Boc-L-Ala-D-Oxd-OBn and of (b) Boc-(L-Ala-D-Oxd)$_2$-OBn, obtained by inversion of the experimental model. Atoms are drawn as spheres with arbitrary radius. Labels are provided for all N and O atoms, for backbone carbons as well as for C and H atoms relevant to H bonding. Color code: C = dark grey, N = blue, O = red, H = light grey. Intramolecular nonclassical H bonds are represented as yellow dotted lines. Selected interatomic distances (Å) and angles (°): in (a), H1···O5 = 2.290(13), C1-H1···O5 = 121.2(10); in (b), H1···O9 = 2.27, C1-H1···O9 = 119.1, H5···O11 = 2.38, C5-H5···O11 = 112.8.

Figures 5 and 6 and inspection of backbone torsion angles (Tables S5-S7) indeed show that the three compounds adopt similar, partially extended conformations, in agreement with ECD studies. In Boc-L-Ala-D-Oxd-OBn and Boc-(L-Ala-D-Oxd)$_2$-OBn, the angles $\phi(\psi)$ at L-Ala residues span the range -87.4 ÷ -70.3° (147.4 ÷ 173.4°) and correspond approximately to the values found in PPII structure.[47] The conformation at the L-Val and L-Lys residues in **3** (ϕ = -134.3 ÷ -132.2°, ψ = 150.6 ÷ 172.0°) is more reminiscent of peptide β strands. The large $|\psi|$ values at amino acid residues in the three structures reflect the fact that C_α-N and C(O)-N_{Oxd} bonds adopt an *anti* confor-

mation which brings the endocyclic carbonyl oxygen of Oxd in a suitable position to interact with the C_α-H group.

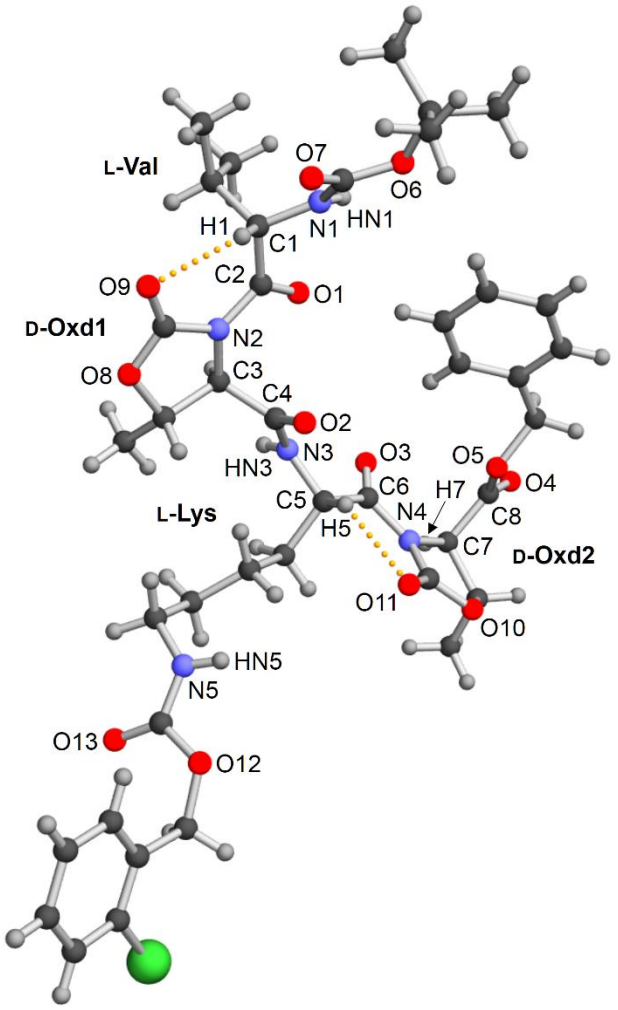

Figure 6. Molecular structure of **3** with atoms drawn as spheres with arbitrary radius. Labelling criteria, H-bond representation and color code are the same as in Figure 5, plus Cl = green. Selected interatomic distances (Å) and angles (°): H1···O9 = 2.28, C1-H1···O9 = 115.0, H5···O11 = 2.32, C5-H5···O11 = 113.5.

Much smaller values would be required to establish a H bond with the N-H group, as found in L-Ala2-D-Oxd2 pair of a similar derivative featuring a different protecting group at the N terminus (ψ = -36.9°).[42]

Because of the structural constraints imposed by the five-membered ring, the $|\phi|$ values at D-Oxd residues span a limited range (64.1 ÷ 81.5°). Omitting the D-Oxd2 residue in **3**, the corresponding $|\psi|$ angles are also similar in the three compounds (-175.7 ÷ -152.0°). The much smaller $|\psi|$ value at the D-Oxd2 residue in **3** (ψ = 20.8°) reflects a *syn* conformation of the OBn termination vs. the C7-N4 bond, as opposed to the *anti* conformation shown by the same structural fragment in Boc-L-Ala-D-Oxd-OBn and Boc-(L-Ala-D-Oxd)$_2$-OBn.

Comparing the capacity of oligomers with different length to accumulate in different cell types provides interesting results. First, the length of the oligomers strongly modulates the capture by any cellular model. While short oligomers weakly interact with cells, **24** and, more intensely, **22** show a clearly improved cell-association capacity already after a 3 h incubation. This outcome could be ascribed to the tendency of **22** and **24** to fold into stable helices, regardless of the presence of positive charges that in principle should favor the cellular uptake. In fact, among the analyzed cells types, monocytes and granulocytes bind these oligomers with best efficacy (6-7 times more effectively than HeLa and lymphocytes). Such a sustained cell capture is still visible after 24 h incubation. This is an interesting possibility in line with our previous works [51,52] in which we demonstrated that only those *Aib*-based foldamers that form a precise helical-spherical domain can target human monocytes, macrophages and dendritic cells more effectively than not-immune cells. Given the different chemical structure of the herein characterized molecules, our new evidence further supports the hypothesis that foldamers with α-helix-like frameworks can favor the binding to inflammatory cells, independently of their charge and chemical nature.

These oligomers may thus be regarded as possible targeting agents of small drugs for several reasons: they are intrinsically non-toxic to cells at relatively high doses; moreover, if long enough, they show a peculiar cell targeting preference, being rapidly and more effectively internalized in human blood myeloid cells, like monocytes and granulocytes. Although the biochemical basis for such cell selectivity, especially displayed by long (> 2 units) and neutral oligomers, has still to be understood, the present formulations or improved analogues may be used to target specific cell types. For example, anti-inflammatory drugs may be coupled to appropriate **18**, **22** or **24** oligomers and directed more selectively to monocytes/granulocytes. Similar foldamers may be refined and serve as alternative targeting agent also for nanoparticles in nanomedicine.

CONCLUSION

Some selected foldamers containing the D-Oxd moiety alternated with a L-amino acid and coupled with Rhodamine-B base have been prepared to check their behavior towards purified human lymphocytes, granulocytes, monocytes and HeLa cells.

The conformational analysis performed in solution and in the solid state suggests that only the longer oligomers of the L-Ala series fold into well-established helices, while the shorter oligomers containing L-Ala and all the oligomers of the cationic series give partially unfolded turn structures. All these molecules show a good biocompatibility, as they show no detrimental effects up to 64 μM concentrations.

A quantitative analysis was obtained by dose and time response analysis by FACS of human HeLa cells, and primary blood lymphocytes, granulocytes and monocytes incu-

bated with foldamers using L-Ala-Piperazine-Rhodamine B as a comparison. Among the analyzed cells types, monocytes and granulocytes bind these oligomers with best efficacy (6-7 times more effectively than HeLa and lymphocytes). Such a sustained cell captured is still visible after 24 h incubation.

The cationic foldamers have a kinetic of cell association slower than what we found for the neutral versions. This outcome could be ascribed to the tendency of **22** and **24** to fold into stable helices, regardless of the presence of positive charges that in principle should favor the cellular uptake.

The bio-compatibility and versatility of these new non-biological oligomers make them a promising base for improvement of drug delivery and for cell selective targeting, as they are intrinsically non-toxic to cells at relatively high doses, and show a peculiar cell targeting preference, being rapidly and more effectively internalized in human blood myeloid cells, like monocyte and granulocytes. Similar foldamers may be refined and serve as alternative targeting agent also for nanoparticles in nanomedicine.

EXPERIMENTAL METHODS

Synthesis. Solvent were dried by distillation before use. All reaction were carried out in dried glassware. The melting points of the compounds are uncorrected. High quality infrared spectra (64 scans) were obtained with an ATR-FT-IR Bruker Alpha System spectrometer. All spectra were measured in solutions at 3 mM concentration in dry CH_2Cl_2 using a 1 mm NaCl cell, or at 1% w/w in dry KBr. All compounds were dried *in vacuo* and all the sample preparations were performed in a nitrogen atmosphere. NMR spectra were recorded with a Varian Inova 400 spectrometer at 400 MHz (^{1}H NMR) and at 100 MHz (^{13}C NMR). The measurements were carried out in D_2O or in $CDCl_3$. The proton signals were assigned by *g*COSY spectra. Chemical shifts are reported in δ values relative to the solvent (D_2O or $CDCl_3$) peak. The 4-carboxy-5-methyl-oxazolidin-2-one (Oxd) was obtained by following the previously reported procedure.[17]

ECD spectra – The ECD spectra were recorded at room temperature on a spectropolarimeter. Quartz cuvettes of 0.2 and 1 mm path length were employed. Foldamers were dissolved in water, yielding clear solutions at approximately 3 mM concentration. The spectra were recorded between 180 and 300 nm for the far-UV and near-UV region, with 0.1 nm resolution. 32 scans were accumulated with a scanning speed of 100 nm/min and a time constant of 1 s and the solvent baseline was subtracted from the averaged spectra. Final spectra are presented in molar ellipticity.

X-ray crystallography. Single-crystal X-ray diffraction studies were carried out at 115(2) K on compounds *rac*-Boc-L-Ala-D-Oxd-OBn (from chloroform), Boc-(D-Ala-L-Oxd)$_2$-OBn (from chloroform) and **3** (from ethyl acetate) with a four-circle Bruker X8-APEX diffractometer equipped with a Mo-Kα generator (λ = 0.71073 Å), an area detector and a Kryo-Flex cryostat, and controlled by Bruker-Nonius X8APEX software. The structures were solved and refined on F_o^2 by standard methods using the WINGX v2013.3 package [53] in conjunction with SIR92 [54] and SHELXL-2014/7 [55] programs. Compound *rac*-Boc-L-Ala-D-Oxd-OBn crystallizes in monoclinic space group $P2_1/n$ (Z = 4) whereas crystals of Boc-(D-Ala-L-Oxd)$_2$-OBn and **3** belong to monoclinic space group $P2_1$ (Z = 2). Disorder effects were limited to the 2Cl-Z substituent in **3**, which was refined over two positions with 0.919(2) and 0.081(2) occupancies. The minority component was restrained to have the same geometry as the majority component within 0.01 and 0.02 Å for 1,2- and 1,3-distances, respectively. Furthermore, its NC(O)O and 2-Cl-Ph moieties were restrained to be flat and all minority atoms were refined with a common isotropic displacement (ID) parameter. All remaining nonhydrogen atoms in the structures were refined anisotropically. Hydrogen atoms were assigned ID parameters but only in *rac*-Boc-L-Ala-D-Oxd-OBn were they subject to unrestrained refinement. Amide hydrogens in Boc-(D-Ala-L-Oxd)$_2$-OBn and **3** were refined independently with N-H distances restrained to 0.880(15) Å and a unique ID parameter in **3**. Aromatic, tertiary and methylene hydrogens in Boc-(D-Ala-L-Oxd)$_2$-OBn and **3** were added in idealized positions and allowed to ride on the parent carbon atom, with U(H) = 1.2U_{eq}(C). Methyl hydrogens were also treated as riding contributors but with torsion angle refinement (AFIX 137), and a common ID parameter *per* CH_3 group in Boc-(D-Ala-L-Oxd)$_2$-OBn or U(H) = 1.5U_{eq}(C) in **3**.

Thanks to the chlorine atom in the partially-disordered 2Cl-Z group, the absolute configuration expected for **3** was confirmed by anomalous dispersion effects using Mo-Kα radiation. In the same conditions, the absolute structure of Boc-(D-Ala-L-Oxd)$_2$-OBn could not be established with certainty, but the Flack parameter (x) suggests that the measured crystal is likely to entail D-Ala and L-Oxd residues, as written (x = -1.4(5) vs. 2.4(5) for the inverted model). CCDC 1493119-1493121 contain the supplementary crystallographic data for this paper. These data can be obtained free of charge from the Cambridge Crystallographic Data Centre via www.ccdc.cam.ac.uk/data_request/cif.

Cell isolation and culture. HeLa cells were maintained in DMEM medium (Gibco) supplemented with 10% FCS (Euroclone) and antibiotics (penicillin and streptomycin, Invitrogen) at 37°C in a humidified atmosphere containing 5% (v/v) CO_2; cells were split every 2-3 days.

Human Monocytes, PMNs and Lymphocytes were purified from Buffy Coats of healthy donors, kindly provided by the Centro Immunotrasfusionale, Hospital of Padova. Briefly, for monocytes purification, buffy coats were subjected to two sequential centrifugations on Ficoll and Percoll gradient (GE Healthcare); residual lymphocytes were removed by incubation in 2% FCS RPMI at 37 °C and subsequently removed by washing. Unless otherwise specified, cells were kept at 37 °C in a humidified atmosphere containing 5% (v/v) CO_2 in RPMI-1640 supplemented with 10% FCS. For granulocytes purification, the pellet of cells obtained after the centrifugation on Ficoll gradient was subjected to dextran erythrocyte precipitation; resid-

ual erythrocytes were removed by hypotonic lysis in 155 mM NH_4Cl, 10 mM $KHCO_3$, and 100 mM Na_2EDTA at pH 7.4 and cells were cultured in RPMI medium, supplemented with 10% FCS. For lymphocytes preparation, buffy coats were incubated with 50 µl/ml of Rosette Sep® Human T Cell Enrichment Cocktail (StemCell Technologies). Blood was then centrifuged over a Ficoll gradient and cells were cultured in RPMI medium, supplemented with 10% FCS.

MTS cytotoxicity assay. HeLa cells (1 x 10^6 cells/ml) were plated into a 96-well culture plate the day before the experiment. Cells were then incubated for 18 h with different oligomers at different concentrations (up to 50 µM) in DMEM additioned with 10% FCS. Cellular mitochondrial activity (indicator of cellular viability) was evaluated by MTS assay (Promega) according to the instruction manual.

Oligomer binding to cells. Intracellular distribution of labelled-oligomers was assessed by confocal microscopy. Human purified monocytes (2x10^5) were seeded on cover glasses and after 24h they were incubated for 18h at 37°C with oligomers, washed with PBS and directly analyzed by confocal microscopy (Leica SP2). Images were processed using ImageJ software. Alternatively, monocytes, granulocytes, lymphocytes or HeLa cells (2x10^5 cells/well) were incubated with labelled-oligomers for 3 or 24 hours at 37°C. Cell MFI (mean fluorescence intensity) values were obtained by cytofluorimetry (FACSCanto, BD) and analyzed by FACSDiva Software (BD).

ASSOCIATED CONTENT

Supporting Information. The Supporting Information file contain: detailed synthesis and characterization of compounds **1-21** and the related NMR spectra; titration curves of compounds **3**, **5**, **7**; ROESY spectrum of compound **7**; crystal data, refinement parameters, hydrogen bonds, selected torsion angles and ORTEP of compound **3**; confocal analysis of human monocytes; association of Rhodamine dye with different human cells.
This material is available free of charge via the Internet at http://pubs.acs.org.

AUTHOR INFORMATION

Corresponding Author

* claudia.tomasini@unibo.it, * acornia@unimore.it,
* regina.tavano@unipd.it

Author Contributions

The manuscript was written through contributions of all authors. / All authors have given approval to the final version of the manuscript.

REFERENCES

(1) Wombacher, R.; Cornish, V. W. *J. Biophotonics* **2011**, *4*, 391–402.
(2) Beija, M.; Afonso, C. a M.; Martinho, J. M. G. *Chem. Soc. Rev.* **2009**, *38*, 2410–2433.
(3) Rad-Malekshahi, M.; Lempsink, L.; Amidi, M.; Hennink, W. E.; Mastrobattista, E. *Bioconjug. Chem.* **2016**, *27*, 3–18.
(4) Horne, W. S.; Gellman, S. H. *Acc. Chem. Res.* **2008**, *41*, 1399–1408.
(5) Gellman, S. H. **1998**, *31*, 173–180.
(6) Bechara, C.; Sagan, S. *FEBS Lett.* **2013**, *587*, 1693–1702.
(7) Shankar, S. S.; Benke, S. N.; Nagendra, N.; Srivastava, P. L.; Thulasiram, H. V; Gopi, H. N. *J. Med. Chem.* **2013**, *56*, 8468–8474.
(8) Fahs, S.; Patil-sen, Y.; Snape, T. J. **2015**, 1840–1853.
(9) Bautista, A. D.; Craig, C. J.; Harker, E. A.; Schepartz, A. *Curr. Opin. Chem. Biol.* **2007**, *11*, 685–692.
(10) Brodsky, B.; Thiagarajan, G.; Madhan, B.; Kar, K. *Biopolymers* **2008**, *89*, 345–353.
(11) Tomasini, C.; Angelici, G.; Castellucci, N. *European J. Org. Chem.* **2011**, 3648–3669.
(12) Lucarini, S.; Tomasini, C. *J. Org. Chem.* **2001**, *66*, 727–732.
(13) Zanna, N.; Milli, L.; Secco, B. Del; Tomasini, C. *Org. Lett.* **2016**, *18*, 1662–1665.
(14) Tomasini, C.; Trigari, V.; Lucarini, S.; Bernardi, F.; Garavelli, M.; Peggion, C.; Formaggio, F.; Toniolo, C. *European J. Org. Chem.* **2003**, *4*, 259–267.
(15) Tomasini, C.; Luppi, G.; Monari, M. *J. Am. Chem. Soc.* **2006**, *128*, 2410–2420.
(16) Angelici, G.; Luppi, G.; Kaptein, B.; Broxterman, Q. B.; Hofmann, H. J.; Tomasini, C. *European J. Org. Chem.* **2007**, 2713–2721.
(17) Luppi, G.; Soffrè, C.; Tomasini, C. *Tetrahedron Asymmetry* **2004**, *15*, 1645–1650.
(18) Mowery, B. P.; Lee, S. E.; Kissounko, D. a.; Epand, R. F.; Epand, R. M.; Weisblum, B.; Stahl, S. S.; Gellman, S. H. *J. Am. Chem. Soc.* **2007**, *129*, 15474–15476.
(19) Sameiro, M.; Gonçalves, T. *Chem. Rev.* **2009**, *109*, 190–212.
(20) Agarwal, N.; Srivastava, P.; Raghuwanshi, S. K.; Upadhyay, D. N.; Sinha, S.; Shukla, P. K.; Ji Ram, V. *Bioorganic Med. Chem.* **2002**, *10*, 869–874.
(21) Haug, B. E.; Stensen, W.; Kalaaji, M.; Rekdal, Ø.; Svendsen, J. S. *J. Med. Chem.* **2008**, *51*, 4306–4314.
(22) Palladino, P.; Stetsenko, D. A. *Org. Lett.* **2012**, *14*, 6346–6349.
(23) Yang, J.; Gellman, S. H. *J. Am. Chem. Soc.* **1998**, *120*, 9090–9091.
(24) Belvisi, L.; Gennari, C.; Mielgo, A.; Potenza, D.; Scolastico, C. *European J. Org. Chem.* **1999**, 2, 389–400.
(25) Kopple, K. D.; Ohnishi, M.; Go, A. *Biochemistry* **1969**, *8*, 4087–4095.
(26) Stevens, E. S.; Sugawara, N.; Bonora, G. M.; Toniolo, C. *J. Am. Chem. Soc.* **1980**, *102*, 7048–7050.
(27) Imperiali, B.; Moats, R. A.; Fisher, S. L.; Prins, T. J. *J. Am. Chem. Soc.* **1992**, *114*, 3182–3188.
(28) Toniolo, C.; Formaggio, F.; Woody, R. W. *Compr. Chiroptical Spectrosc. Vol. 2 Appl. Stereochem. Anal. Synth. Compd. Nat. Prod. Biomol.* **2012**, *2*, 499–543.
(29) Venkatachalam, C. M. *Biochim. Biophys. Acta* **1968**, *168*, 411–416.
(30) Toniolo, C.; Formaggio, F.; Tognon, S.; Broxterman, Q. B.; Kaptein, B.; Huang, R.; Setnicka, V.; Keiderling, T. a.; McColl, I. H.; Hecht, L.; Barron, L. D. *Biopolymers* **2004**, *75*, 32–45.
(31) Toniolo, C.; Polese, a; Formaggio, F.; Crisma, M.; Kamphuis, J. *J. Chem. Soc. Chem. Commun.* **1996**, *118*, 2744–2745.
(32) Manning, M. C.; Woody, R. W. *Biopolymers* **1991**, *31*, 569–586.
(33) Matthews, B. W. *Protein Sci.* **2009**, *18*, 1135–1138.
(34) Hague, D. E.; Idle, J. R.; Mitchell, S. C.; Smith, R. L. *Xenobiotica* **2011**, *41*, 837–843.
(35) Cai, W.; Marciniak, J.; Andrzejewski, M.; Katrusiak, A. *J. Phys. Chem. C* **2013**, *117*, 7279–7285.

(36) Faigl, F.; Fogassy, E.; Nògràdi, M.; Pàlovics, E.; Schindler, J. *Tetrahedron Asymmetry* **2008**, *19*, 519–536.
(37) Pellegrini, M.; Wukovitz, S. W.; Yeates, T. O. *Proteins* **1997**, *28*, 515–521.
(38) Yeates, T. O.; Kent, S. B. H. *Annu. Rev. Biophys.* **2012**, *41*, 41–61.
(39) Mandal, P. K.; Collie, G. W.; Kauffmann, B.; Huc, I. *Angew. Chem. Int. Ed.* **2014**, 14424–14427.
(40) Pentelute, B. L.; Gates, Z. P.; Tereshko, V.; Dashnau, J. L.; Vanderkooi, J. M.; Kossiakoff, A. A.; Kent, S. B. H. *J. Am. Chem. Soc.* **2008**, *130*, 9695–9701.
(41) Saha, I.; Chatterjee, B.; Shamala, N.; Balaram, P. *Biopolym. - Pept. Sci. Sect.* **2008**, *90*, 537–543.
(42) Fanelli, R.; Milli, L.; Cornia, A.; Moretto, A.; Castellucci, N.; Zanna, N.; Malachin, G.; Tavano, R.; Tomasini, C. *European J. Org. Chem.* **2015**, *2015*, 6243–6248.
(43) Milli, L.; Larocca, M.; Tedesco, M.; Castellucci, N.; Ghibaudi, E.; Cornia, A.; Calvaresi, M.; Zerbetto, F.; Tomasini, C. *J. Org. Chem.* **2014**, *79*, 5958–5969.
(44) Luppi, G.; Galeazzi, R.; Garavelli, M.; Tomasini, C. **2004**, *3*, 2181–2187.
(45) Angelici, G.; Falini, G.; Hofmann, H.-J.; Huster, D.; Monari, M.; Tomasini, C. *Angew. Chemie Int. Ed.* **2008**, *47*, 8075–8078.
(46) Angelici, G.; Falini, G.; Hofmann, H. J.; Huster, D.; Monari, M.; Tomasini, C. *Chem. - A Eur. J.* **2009**, *15*, 8037–8048.
(47) Longhi, G.; Abbate, S.; Lebon, F.; Castellucci, N.; Sabatino, P.; Tomasini, C. *J. Org. Chem.* **2012**, *77*, 6033–6042.
(48) Kirkham, S.; Hamley, I. W.; Smith, A. M.; Gouveia, R. M.; Connon, C. J.; Reza, M.; Ruokolainen, J. *Colloids Surfaces B Biointerfaces* **2016**, *137*, 104–108.
(49) Lohse, J.; Nielsen, P. E.; Harrit, N.; Dahl, O. *Bioconjug. Chem.* **1997**, *8*, 503–509.
(50) Nguyen, T.; Francis, M. B. *Org. Lett.* **2003**, *5*, 3245–3248.
(51) Rio-Echevarria, I. M.; Tavano, R.; Causin, V.; Papini, E.; Mancin, F.; Moretto, A. *J. Am. Chem. Soc.* **2011**, *133*, 8–11.
(52) Tavano, R.; Malachin, G.; De Zotti, M.; Peggion, C.; Biondi, B.; Formaggio, F.; Papini, E. *Biochim. Biophys. Acta - Biomembr.* **2015**, *1848*, 134–144.
(53) Farrugia, L. J. *J. Appl. Crystallogr.* **2012**, *45*, 849–854.
(54) Altomare, A.; Cascarano, G.; Giacovazzo, C.; Guagliardi, A. *J. Appl. Crystallogr.* **1993**, *26*, 343–350.
(55) Sheldrick, G. M. *Acta Crystallogr. Sect. C Struct. Chem.* **2015**, *71*, 3–8.

Insert Table of Contents artwork here